Aurivillius-Phase Bi4Ti3O12-nBiFeO3 Materials

Subjects: Others

Contributor: Shu-jie Sun

Aurivillius-type layered compound have attracted increasing research interest, especially in recent 20 years, due to their promising electrical properties as new lead-free piezoelectric materials operating at high temperatures. For instance, the well-known Bi4Ti3O12, presents large spontaneous polarization, anisotropy and high ferroelectric Curie temperature and have wide applications in the electronic industry, capacitors, transducers, nonvolatile ferroelectric memories, piezoelectric sensors and optical devices. To increase functionality of Bi4Ti3O12 modification with BiFeO3 is very promising, which is also a methodology for constructing single-phase multiferroics in which ferrelectricity and magnetic ordering are coupled near room temperature. Combining these two materials exhibiting different physical performances one can create a kind of novel materials and thus achieve functionality. Herein, we summarized the recent progress in the field of synthesis of BFTO-n materials with various architectures and highlighted their extraordinary properties for promising applications in the electronic industry, quantum devices, capacitors, transducers, microwave absorbers, catalysts and photoelectric devices.

Aurivillius Layered oxides multiferroic BiFeO3 Ferroelectric

1. Introduction

It is commonly known that the $Bi_{n+1}Fe_{n-3}Ti_3O_{3n+3}$ (BFTO-*n*) compounds of binary $Bi_4Ti_3O_{12}$-$BiFeO_3$ system combine FE, magnetic and ME properties, making the potentially attractive for producing advanced materials for information processing and storage applications. More intriguingly, such oxides exhibit important characteristics as follows: i) structure breaks the spiral spin canting superposed onto the G-type antiferromagnetic order as well as can accommodate different magnetic ions realizing strong magnetic interactions; ii) the origin of the ferroelectricity is a combination of oxygen octahedral rotations and polar distortions; iii) different layer numbers in the perovskite slabs show a larger difference on physical properties.

2. Basic structure and Morphology

2.1. Aurivillius-Phase Layered Structure

The BFTO-n oxides are layered perovskite structures, in which fluorite-like Bi-O layers alternate with *n* perovskite-like layers. Figure 1a shows the prototype of the Aurivillius-phase structure as a function of the number of perovskite layers. The layered compounds form a natural structural-stack and, ideally, form as a single-phase. In the limiting case $n = \infty$, the repeated cell is the pure perovskite and can be regarded as a structure of $BiFeO_3$,

which has a rhombohedral distorted perovskite unit cell. The atomic-scale layered structure of the BFTO-*n* oxides can be visualized by the state-of-the-art aberration corrected scanning transmission electron microscopy high angle annular (STEM-HAADF) image carried out on scanning transmission electron microscope, as shown in Figure 1b. In the STEM-HAADF image, the orderly arranged bright spots all belong to the Bi atoms, and four layers of Bi atoms (Ti/Fe atoms are neatly arranged between layers) sandwiched by two closely stacked Bi layers (namely the fluorite-type Bi-O layers) can be understandable as corresponding to 5-layer perovskite slabs, which presents typical Aurivillius-type layered structures.

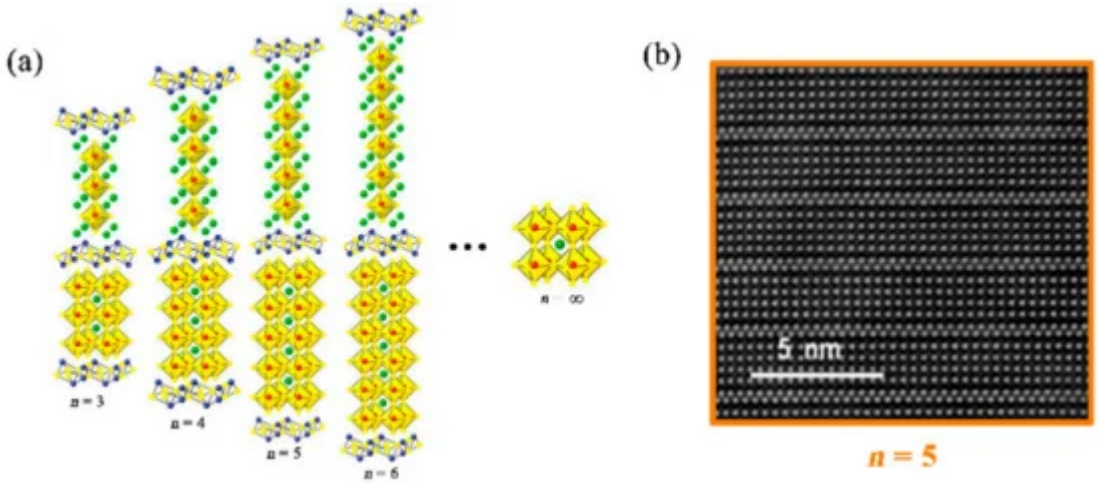

Figure 1. (**a**) Prototype of Aurivillius-type structure for the BFTO-*n* as a function of the number of layers (examples of each case are $Bi_4Ti_3O_{12}$, $Bi_5FeTi_3O_{15}$, $Bi_6Fe_2Ti_3O_{18}$, and $Bi_7Fe_3Ti_3O_{21}$); (**b**) scanning transmission electron microscopy high angle annular (STEM-HAADF) image of the BFTO-5 as an example. The orderly arranged bright spots in the STEM-HAADF image all belong to the bismuth atoms.

Up to now, the single-phase BFTO-*n* compounds with integer $n \leq 9$ have been synthesized by using the different methods, whereas the synthesis of the pure compounds with $n > 9$ are still a big challenge, due to kinetic or thermodynamic reasons and produced reaction intermediates or impurity phase. Of particular interest is that *n* may take fractional values, confirmed by some works. The compounds with fractional *n* have a mixed-layer structure alternating perovskite layers of different thicknesses. For examples, $Bi_{11}Fe_3Ti_6O_{33}$, is made up of alternating $n = 4$ and 5 perovskite layers, so that the average number of its perovskite layers per unit cell is $n = 4.5$. It should be emphasized that the mixed-layer structure is disorder rather than order in most cases. The difference of the order and disorder Aurivillius-type intergrowths are shown in Figure 2.

To elucidate mechanisms for the compound formation with various perovskite slabs and obtain new compounds including mixed-layer structure in the $Bi_4Ti_3O_{12}$-$BiFeO_3$ system, in earlier research, major attention was paid to structure and thermal behavior and researchers from Russian Academy of Sciences. All of the BFTO-*n* compounds were found to have orthorhombic structures. Analysis of phase changes for the compounds with different *n* can reveal a number of general trends: 1) with increasing *n*, the peak occurring at 15°–20° shifts toward the higher angle while the peak at 30°–35° shifts toward lower angle, the peak spacing between two peaks at 45°–50° gradually become larger, and two peaks separated clearly at 50°–55° gradually overlap each other; 2) As *n*

increases, the *c* cell parameter rises almost linearly, the best fit straight line $c = 8.22n + 8.16$ and the average thicknesses of one perovskite layer and the fluorite-like layer is 4.11Å and 4.08 Å, respectively ; 3) The compounds are close in chemical composition and subject to the general tendency, as a rule, the degree of ordering in the layer stacking can be assessed for new materials with fractional *n* values. In addition, recent studies found an abrupt decrease in the temperature of their decomposition when $n > 6$, possibly caused by thermal instability of $BiFeO_3$ (exceeds 70 mol %) in considered temperature range. Moreover, the BFTO-*n* compounds at $n > 6$ are distinguished by the slight differences in the solidus and liquidus temperatures, being in a state close to indifferent equilibrium. This noteworthy feature correlates with considerable structural alterations in them at $n > 6$. In a word, the high $BiFeO_3$ percentages and the abrupt decrease in the thermal stability affect the stability of the BFTO-*n* ($n > 6$), probably resulting in the occurrence of the complicated mixed-layer structure.

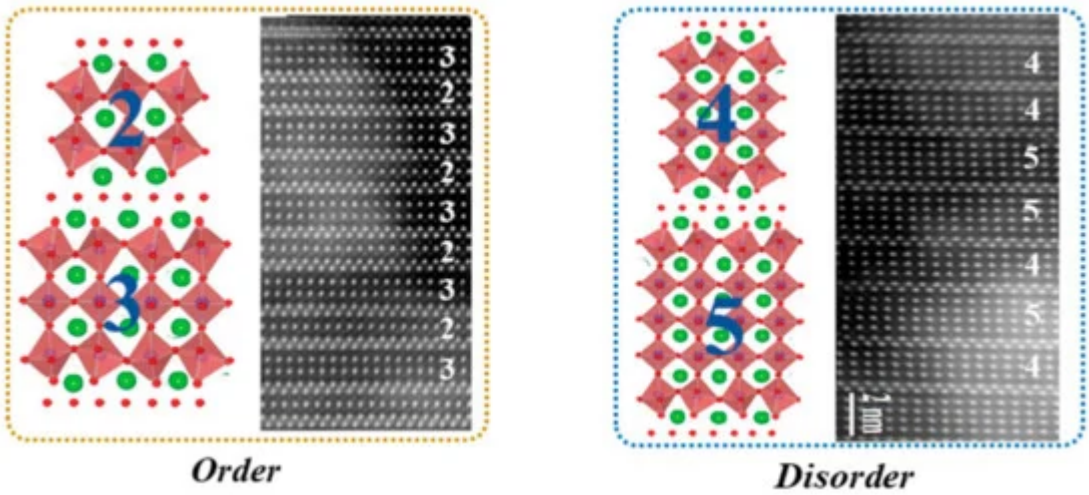

Figure 2. Aurivillius-type intergrowths: Order and Disorder. Examples of the Order and Disorder are $n = 2$ and 3 for $Bi_7Ti_4NbO_{21}$, and $n = 4$ and 5 for $Bi_{11}Fe_3Ti_6O_{33}$, respectively.

2.2. Controllable Synthesis and Morphological Features

The main approaches to making BFTO-*n* materials include the conventional solid state reaction method, sol-gel method or chemical solution deposition method or Pechini's method, coprecipitation method, hydrothermal synthesis method, molten salt method, and micro-pulling down method. The general pathways of these methods are present in Figure 3.

2.2.1. Ceramics

Layer-structure determines the growth habit for the BFTO-*n*. They grow with anisotropic shapes, as platelets with the minor dimension in parallel to the *c*-axis. This is a disadvantage for the sintering process to obtain dense bulk ceramics but it favors the grain alignment that allows the texture and the crystal orientation, as shown in Figures 4a–4c, carried out by different means, such as hot pressing, tape-casting, template grain growth or others. Because of lower cost and the possibility of obtaining high amount of materials, the ceramic method is the most used route for the processing of materials with Aurivillius structure. However, a major drawback for this method is

that the lamellar crystal growth makes the compaction of precursor ceramic powder more difficult. The reduced mass transport during sintering easily led to porous ceramics, higher than ~10 % of porosity. Fabrication of the BFTO-*n* ceramics generally follows the procedures of pre-sintering for powders and sintering of the hot/cold-pressed green pellets.

2.2.2. Thin films

In order to drive device applications, the BFTO-*n* materials in the form of thin films are required. Currently, polycrystalline BFTO-*n* thin films were successfully prepared by typical chemical solution deposition method or sol-gel method, which consists of the solution preparation and spin coating processing. The practical substrate usually adopts the Pt/Ti/SiO_2/Si substrate, fused quartz substrate, sapphire substrate, and so on. Figures 4d and 4e shows the field emission scanning electron microscope (FE-SEM) images of surface and fracture morphologies of the BFTO-*n* thin film. Yet, owing to the almost equal Gibbs free energies and the increased inner constraint of crystalline structures, it is difficult to synthesize BFTO-*n* ($n > 6$) with a homogeneous layer-structure by using the existing methods. The fabrication of single crystal epitaxial thin films of the BFTO-*n* has been a long-standing challenge due to their thermodynamic phase-instability and the large stacking layer number. Through the long-continued efforts, little work has been done on the high-quality single-crystalline BFTO-*n* thin films. For example, BFTO-8 epitaxial films were obtained on TiO_2-terminated $SrTiO_3$ (001) substrates using pulsed laser deposition with a KrF excimer laser ; the epitaxial growth of BFTO-5 on $(LaAlO_3)_{0.3}(Sr_2AlTaO_6)_{0.7}$ (LSAT) substrate and $LaNiO_3$ conductive buffer layer was done, using laser molecular-beam-epitaxy employing a KrF excimer laser.

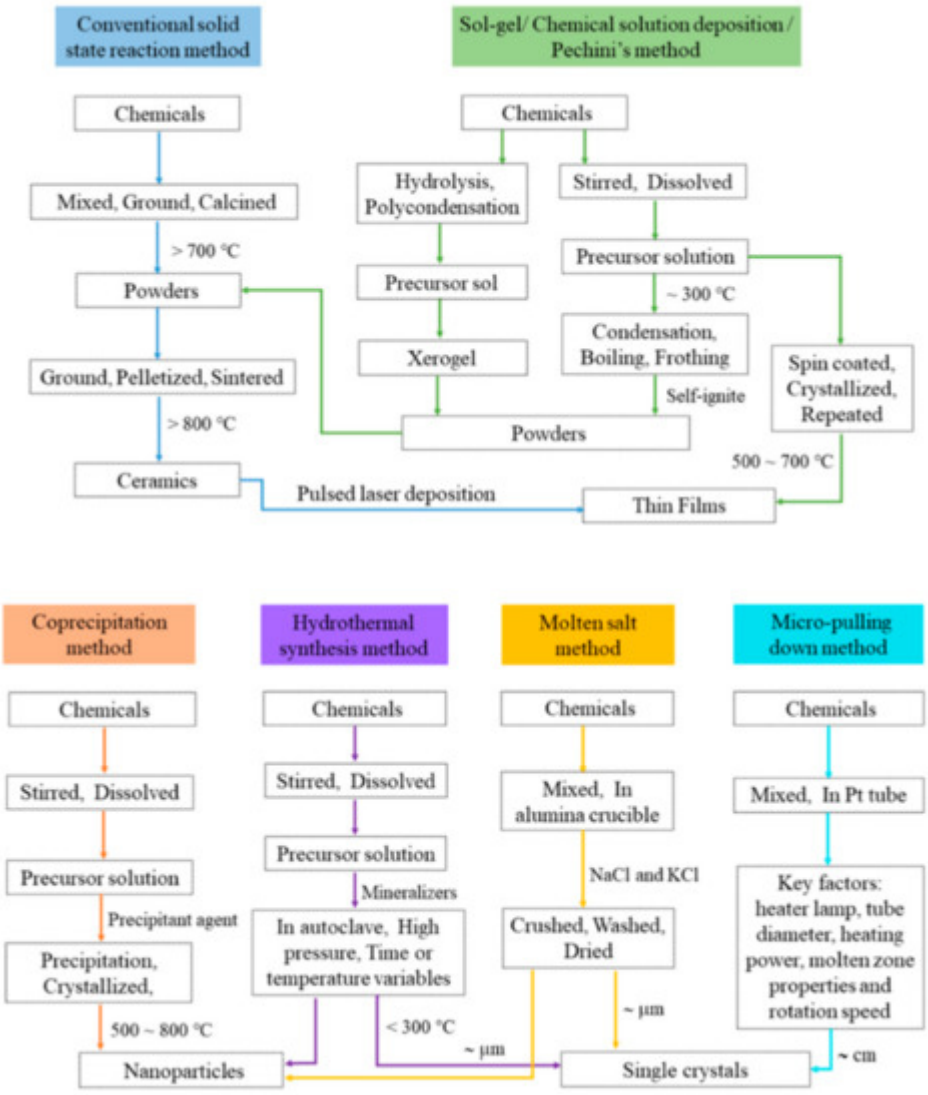

Figure 3. General pathways of different synthesized methods for the BFTO-*n* materials. .

2.2.3. Nanostructures and Single crystals

Because of specific surface effect, small size effect, quantum effect, *etc.*, the nano-phase materials show manifold excellent performances and have broad applications in the fields of environmental pollution and shortage of clean energy. So, the BFTO-*n* in the form of nanostructure attracted extensive attention worldwide in recent years and diverse nanostructures of them including nano-shelves, nano-belts, nano-fibers, nano-sheets, nano-plates, and nano-flowers were synthesized and applied as catalysts for photo-degradation, visible-light-driven water splitting, and oxygen evolution reaction. Morphology of the BFTO-*n* nanobelts synthesized via electrospinning is shown in Figure 4e. These nanobelts present belt morphology with well-developed crystallization, but the belts could become rougher with the size of particles and pores increased with increasing the calcination temperature. The BFTO-4 nanoflowers and truncated tetragonal bipyramid BFTO-4 nanoplates are shown in Figures 4f and 4g, respectively. In fact, the previous work found that various morphologies such as nanoflowers, nanosheets, and microplates can be synthesized successfully by a hydrothermal method adopted different operate technology and process. The concentration of MOH (Na^+ or/and K^+) solution as mineralizer and citrate acid as adjuvant play a

critical role for the morphology control of the nanostructure. Whatever hierarchical morphology stacked by regular nanosheets or individually crystalline nanoplates, there are some different exposed facets which may produce different numbers of reactive sites and carrier migration ability, thus presenting diversified physicochemical performances. The selected area electron diffraction (SAED) patterns taken from four corns of one BFTO plate from the sample in Figure 4h exhibit almost identical diffraction spots corresponding to (200) and (020) plane, confirming the single-crystalline nature (Figure 4i). More importantly, this individual single-crystalline nanoplate can verify intrinsic FM and FE properties of Aurivillius-type BFTO-*n* compounds. Apart from the nano-crystals, single crystals of the BFTO-*n* were grown by using modified micro-pulling down method. The growth system uses mirror halogen lamps and a Pt tube, and the type of heater lamp, tube diameter, heating power, molten zone properties, and rotation speed are key factors and should be adjusted for different crystal types.

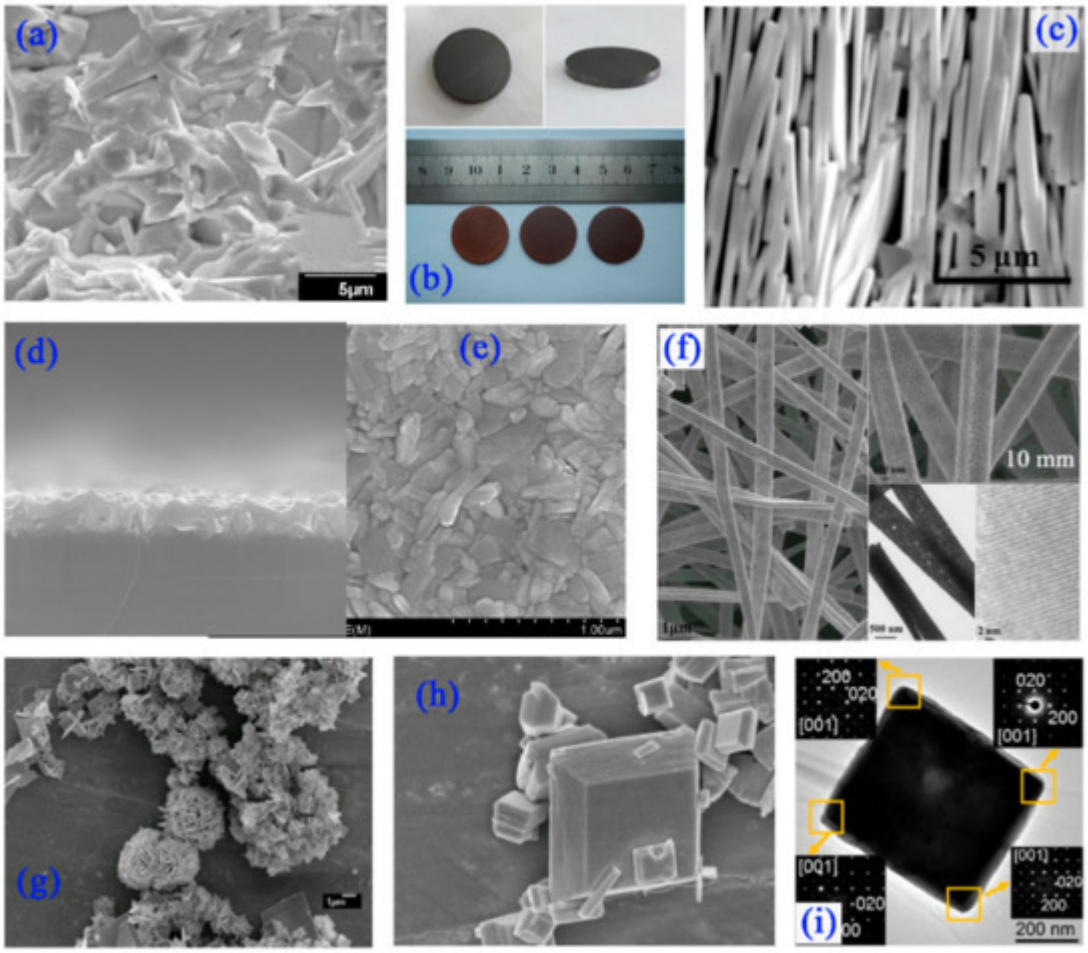

Figure 4. (a) SEM image of BFTO-6 ceramic from fresh fracture surface. (b) The photo of hot-pressed BFTO-6 ceramics. (c) Cross-section SEM images of BFTO-6 ceramic prepared by dry pressing the nanoplates and subsequently sintering without pressure. The FE-SEM images of (d) surface and (e) cross-sectional morphologies of BFTO-4 thin film on (111) Pt/Ti/SiO_2/Si substrate. (f) SEM, TEM, and HRTEM images of the BFTO-8 nanobelts. SEM images of (g) BFTO-4 nanoshelf or nanoflower and (h) individual BFTO-4 nanoplate. (i) TEM image of BFTO-4 plate on the ab plane.

3. Extraordinary Properties and Potential Applications

3.1. ME Coupling

ME coupling is one of the most appealing aspects of multiferroics, because it provides additional degrees of freedom for manipulating the polarization/magnetization in multifunctional devices, such as actuators, sensors, and data storage devices [4]. Coupling between electric and magnetic dipoles at RT was demonstrated by i) measuring the effects of electric poling on magnetic hysteresis loop or vice versa; ii) directly measuring the value of ME voltage coefficient a_{ME} using a ME coupling test system; iii) visualization of magnetic/electric-field-induced FE/FM domains switching by piezoresponse force microscopy (PFM); iv) measuring the change in dielectric constant under an applied magnetic field. The BFTO-*n* materials were deemed as potential RT single-phase multiferroics, including large FE and FM properties, high FE and FM transition temperatures, and a ME coupling that occurs at or above the RT together with the ability to be driven as an external electric or magnetic field as possible.

ME coefficient of the BFTO-4 was ~ 17 $mVOe^{-1}cm^{-1}$ at 8 kOe, and the BFTO-5 was only ~3.2 $mVOe^{-1}cm^{-1}$ at 4 kOe. When $n > 6$, the ME interaction is very weak and nearly undetectable [184]. Moreover, the coupling coefficient in single-phase $BiFeO_3$, as reported firstly by Ismailzade's group (1979), was rather small but measurable, only 0.064 $mVOe^{-1}cm^{-1}$ at 9.5 kOe. This seems to mean that as the Fe content increases, the ME interaction in the $Bi_4Ti_3O_{12}$-$BiFeO_3$ system decreases, thereby affecting the ME coefficient. Recently, some attempts were made to enhance the ME coupling in the BFTO-*n* by: i) chemical substitution with rare earth elements at A-site; ii) construction of nanosized bulk composites or film heterostructures; and iii) development of nanoparticle or nano-fibers via various chemical routes.

A maximum a_{ME} as high as ~ 400 $mVOe^{-1}cm^{-1}$ at RT was obtained in the BFTO-4 thin film, the BFTO-4/NBT composite thin films or pseudo1-3 type FeGa/BFTO-4 hetero-structural films. However, the ME coefficient of the BFTO-*n* materials is still inferior, compared with the bulk ME composites with a_{ME} up to several $VOe^{-1}cm^{-1}$ for technological application as the ME devices. Therefore, there is still a large scope to improve ME coefficient. Perhaps forming composite films or nanocomposites consisting of a strong magnetic phase and piezoelectric phase with high piezo-response, structural architecture, and layer or interface engineering, and so on, may lead to a high ME coefficient.Although the ME coefficient matters, the deterministic control of FE domains by magnetic field or control of magnetic domains by electric field is perhaps more critical to realize the practical device applications. In $BiFeO_3$-based multiferroics, this research topic has attracted tremendous research interests over the past few years and most of relevant works focusing on $BiFeO_3$/ $La_{0.7}Sr_{0.3}MnO_3$ or $BiFeO_3$/$Co_{0.9}Fe_{0.1}$ have been comprehensively summarized in some excellent review papers. For BFTO-*n*, a direct evidence of the ME coupling was sought by performing PFM under a variable magnetic field to locally image any coupled piezoelectric-magnetic switching. Single-frequency PFM was performed on the $Bi_6Ti_{2.99}Fe_{1.46}Mn_{0.55}O_{18}$ thin film and the influence of a full magnetic field step cycle on the FE domains was investigated, see Figure 5a. Two distinct types of FE domains behavior could be observed as demonstrated by regions of the sample circled in green and yellow in amplitude and phase images. It is evident that field-dependent

reversible ME coupling behavior is observed for the yellow circles. Its feature is as follow: the magnitude of piezo-response and the size of domain increases on an increase in magnetic field to +2500 Oe and disappears on reversal of the magnetic field to 0 Oe, then the domain is again generated on a decrease in magnetic field to –2500 Oe and disappears again on reversal of the magnetic field to 0 Oe. The irreversible domain switching is also observed for the green circles, which shows that the piezoelectric domain emerges and grows but does not disappear under a variable magnetic field. More importantly, Jia *et al.* demonstrated the availability of the manipulation of magnetic domains by electric field in the BFTO-4 film at RT, see Figure 5b. A sharp contrast in the magnetic domains indicates magnetic domains in the BFTO-*n* film can be switched by the electric field. After removing the electric field for 22 h, the switched magnetic pattern nearly fades away, suggesting the E-switched magnetic domains are coupled to ferroelastic domains, caused by a short-range magnetic ordering status and unstable magnetoelastic coupling.

In a nutshell, both FE and magnetic domain switching behavior in BFTO-*n* multiferroic materials show the coupling between electric dipoles and magnetic orderings, and provide the possibility of manipulating one physical parameter by using one of the external stimuli, such as magnetic field, electrical field, and so on, which could yield an additional degree of freedom in novel multi-functional device design. We believe that these findings will give a great push to realize the practical single-phase RT ME device applications.

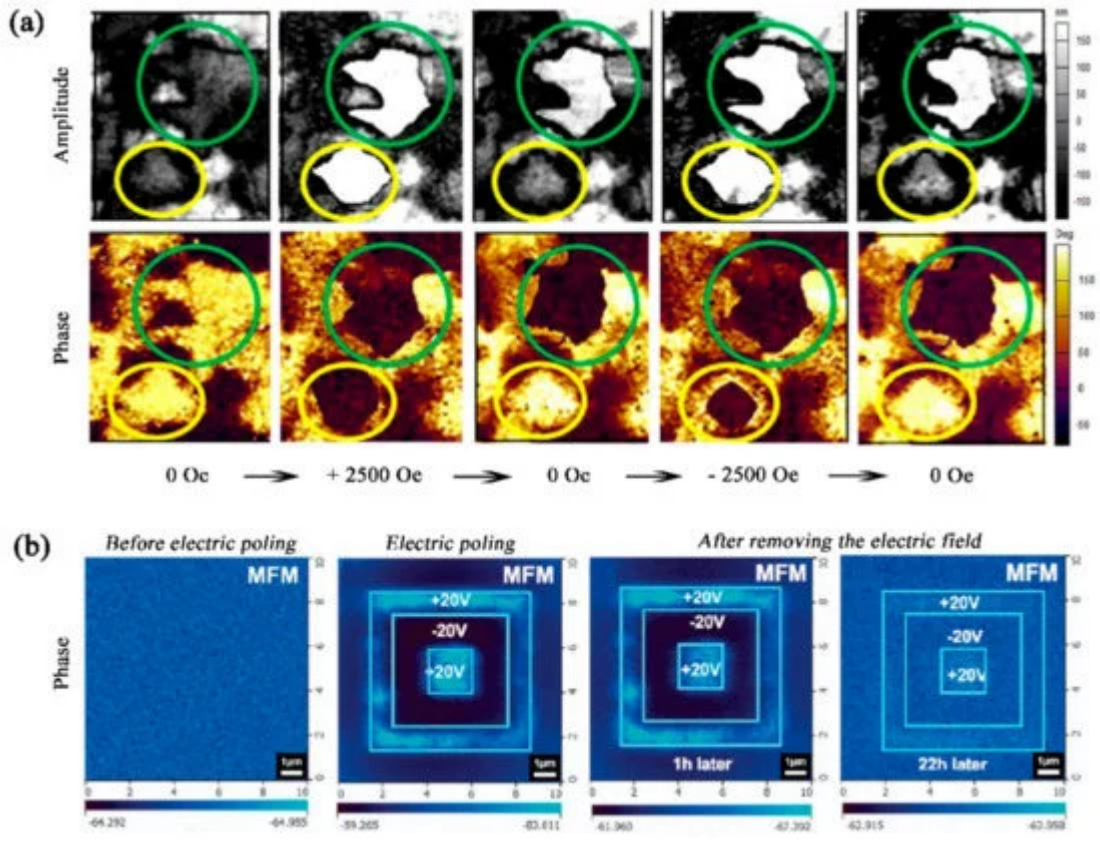

Figure 5. (a) Control of electric domains by magnetic field. Representative images of the effect of a complete magnetic field cycle applied locally to the $Bi_6Ti_{2.99}Fe_{1.46}Mn_{0.55}O_{18}$ thin film on the in-situ in-plane lateral

piezoresponse force microscopy measurements. The images demonstrate magnetic-field-induced irreversible (green circles) and reversible (yellow circles) ferroelectric domain nucleation and saturation under the magnetic field cycle. (b) Control of magnetic domains by electric field. Magnetic force microscope (MFM) phase images of the $Bi_5FeTi_3O_{15}$ thin film before electric poling, electric poling by +20 V in the area of 7 × 7 μm^2, −20 V in 5 × 5 μm^2, and + 20 V in 2 × 2 μm^2, with reading over 10 × 10 μm^2, and after removing the electric field for 1 and 22 h.

3.2. Exchange Bias

Exchange bias (EB) generally manifests itself as a shift of the magnetization hysteresis loop along the magnetic field axis when the system is cooling down fully through its Neel temperature under an external magnetic field. This EB effect plays a crucial role in developing fundamental physics as well as applications of magnetic tunnel junctions and spintronics. The EB effect was usually observed in a variety of artificial materials, such as superlattices, heterogeneous, and core-shell nanoparticles consisting of FM and AFM components. However, the RT EB effect for most materials greatly hinders their potential applications as devices. As an early stage effort, recently, the research has been to focus on the single-phase EB materials. Unfortunately, till now, the EB materials with single-phase are still rare and the observed single-phase EB behaviors were still limited by the small exchange-bias field and the low reachable operation temperatures.

In this BFTO-*n* system, those short-period compounds have paramagnetic ground state at RT, while those long-period compounds ($n > 6$) are mostly AFM materials with a weak FM at RT. Appearance of this weak FM could trigger the formation of spin glassy magnetic states, based on the coexisted FM and AFM interactions, and may induce EB effect. It was found that there is good EB behavior in the BFTO-7, BFTO-8, and BFTO-9. However, the detected bias temperatures, usually at 10~250 K below freezing temperatures (T_f) of spin glass transition, are all below RT. Surynarayana *et al*. found that the T_f in the BFTO-*n* increases with their layer number *n*. If so, the BFTO-9 has a T_f ~280 K and the anticipated EB temperature for the BFTO-*n* with $n \sim 10$ may be close to RT, but, in fact, it is very difficult to synthesize such oxides because of their almost identical formation energies and more fragile stacked structures. A new strategy instead of merely increasing the layer numbers n was proposed by a simple Fe/Ti mole ratio modulation in the BFTO-9. Consequently, the Neel temperature and T_f of the samples can reach above RT and the RT EB behavior was successfully realized in $Bi_{10}Fe_{6.4}Ti_{2.6}O_{30+d}$ with a maximum EB field (H_{EB}) of approximately ~38 Oe. In addition, the anisotropy of the EB effect was found in bismuth-based layered oxyhalides, for example a 4-layer $Bi_7Fe_2Ti_2O_{17}Cl$.

Normally, EB effect denotes the horizontal shift of the FM hysteresis loop after proper magnetic FC to below the ordering temperature of the AFM component. For a single-phase ME material with AFM property, the ME-based switching EB effect from the system consisting of a FM multilayer on top of this ME single crystal was reported. The switching mechanism is based on the so-called ME field (*e.g.,* electric field) cooling process, which favors the growth of a distinct AFM single domain and thus an efficient control of the AFM interface moment whose sign is decisive for that of H_{EB}. For example, Cr_2O_3 (0001) and a FM Co/Pd multilayer film. In the EB system, a reversible and global electric switching of the EB field was realized isothermally at RT. If a simple single-phase ME material with good RT EB effect can add a new regulating factor for EB through the use of an electric field, it will promise

applicability in future ME devices. Unfortunately, electrically controlling EB in BFTO-n was barely reported until now. A great deal of research, therefore, is urgently needed. Further, it will be interesting and open new possibilities, if the electric control of EB effect in single-phase BFTO-n at RT can be realized.

3.3. Microwave Absorption

Design and development of novel high efficiency microwave absorbing materials and bringing these materials into practical use, such as healthcare, signal protection, and national defense security, are always important. Magnetic ferrite and carbon-based nanocomposites have been widely explored as two attractive candidates for microwave absorption; however, complex fabrication, relatively low output capacity, high density, and so on, limit their applications. In fact, both electric and magnetic dipoles are strong absorbers of microwave. Dielectric-magnetic compositing is an effective strategy to enhance microwave attenuation. Recently, single-phase RT multiferroics are increasingly studied as candidates for eliminating electromagnetic waves. Some types of multiferroics, *e.g.,* $BiFeO_3$, YIG, and hexaferrite, were developed as microwave absorbing materials. Wen *et al*. reported a minimum reflection loss (RL) of $BiFeO_3$ as −46 dB at 11.2 GHz and the absorption bandwidth of the RL below −10 dB is about 3 GHz. However, the absorption capacity, bandwidth and thickness of such studied materials still need to be improved further to meet the demand of high efficiency and stabilization. Aurivillius BFTO-*n* can present large dielectric, FE, and FM behaviors and electromagnetic interaction, thus they are likely to be a new type of microwave materials with excellent microwave absorption. Liu *et al*. reported that La-modified $La_xBi_{5-x}Fe_{0.5}Co_{0.5}Ti_3O_{15}$ materials have a microwave absorption. Specifically, the specimen with x = 0.75 delivered a minimum RL of −15.8 dB at a small thickness of 1.8 mm and a broadened absorption bandwidth (≤−10 dB) of 3.0 GHz (9.5–12.5 GHz). In our early work, a larger absorbing intensity and broader absorbing bandwidth in $Bi_7Fe_{2.25}Co_{0.75}Ti_3O_{21}$ was found. The minimum RL surpasses −30 dB at different thick-nesses (1–5 mm) and absorption bandwidth (≤ −20 dB) was close to 12 GHz (5.7–17.7 GHz). Moreover, the microwave absorption property is sensitive to the sample thickness and the electro-magnetic tailor-ability can be manipulated through appropriately designed the thickness. These works highlighted the application of the Aurivillius-type multiferroic oxide materials as smart absorbers in microwave field.

3.4. Photo/Electro-Catalyst Activity

As potential candidates for highly active photo-catalysts, a lot of attention has been given to the BFTO-*n* oxides. The main reasons are as follows: i) the presence of Bi enhances the likelihood of visible-light absorption by pushing up the valence band edge due to the hybridization of Bi 6s with O 2p orbital; ii) largely dispersed hybridized valence band favors the high mobility of the photo-generated holes and is beneficial to the oxidation reaction; iii) materials have narrow and tunable band gaps; iv) spontaneous polarizations may be effective in helping the separation of photon-generated electrons and holes; v) ferromagnetism may be helpful in making recyclable catalysts. Better than the selective TiO_2-based oxides utilizing mostly UV light, the BFTO-*n* materials may act as excellent visible-light-driven photocatalysts, having wide applications not only in environmental remediation, water disinfection, pollutant degradation, air purification, and self-cleaning of surfaces, but also in the area of renewable energy generation in the form of hydrogen by water splitting. Aurivillius-type BFTO-*n* have been

reported as a family of visible-light photocatalysts such as BFTO-4 microflowers, BFTO-5 nanofibers, and BFTO-6 nanoshelf. While most of the studies have only focused on the degradation of a single dye as a pollutant. For example, Naresh *et al*. synthesized La-doped BFTO-4 and found that such oxides exhibited efficient rhodamine B (RhB) degradation under sunlight irradiation. As the wastewater is contaminated with multiple dyes rather than a single dye, it is desirable to test the efficiency of a catalyst toward the collective removal of multiple dyes from a mixture. Naresh *et al*. reported that a series of five-layer $Bi_5AFeTi_4O_{18}$ (A = Ca, Sr, and Pb) compounds not only exhibited collective photocatalytic degradation of RhB-methylene blue and RhB-rhodamine 6G mixture at pH = 2, but also showed almost 100% photo-catalytic selective degradation of methylene blue from the RhB-methylene blue mixture at pH = 11 under natural solar irradiation. In addition, size, morphology, surface area, *etc*., of a catalyst may greatly affect its catalytic performance. The BFTO-*n* nanostructures by morphology control were studies and the synergistic effect of different facets in the separation of electrons and holes and oxidation/reduction reaction were found. Rare-earth ions *f*-orbitals can form complexes with various Lewis bases and affect performance. For example, Eu-doped $Bi_5Fe_{0.95}Co_{0.05}Ti_3O_{15}$. Because of near-infrared light making up about 47% of solar spectrum, the extended utilization of sunlight from ultraviolet and visible light to near-infrared light is an attractive issue for developing photocatalysts. Near-infrared photoactivity of the BFTO-*n* photocatalysts [55,208] were also reported.

Aurivillius-type BFTO-*n* was recently explored as a kind of high-efficiency electrocatalyst for oxygen evolution reaction (OER). OER is the rate-determining step in the electrocatalytic water splitting and both electrical conductivity and absorption capability are the two key factors for its strength. Excitingly, the spontaneous polarization of the FE materials can be taken advantage of to separate the carriers, as well as produce an external screening effect absorbing charged ions and molecules from outside to neutralize their polarization. Therefore, the BFTO-*n* with large FE intrinsic polarization, can be considered as an excellent material matrix to enhance electrical conductivity and adsorption capacity, further to improve the OER efficiency. Two works about the OER efficiency of the BFTO-*n* were recommend: one is that three oxides in $Bi_7Fe_{3-x}Co_xTi_3O_{21}$, all Fe-based (x =0), half-half Fe-Co based (x = 1.5), all Co-based (x =3), were prepared to investigate OER activity; The other work presents a methodology by in-situ growth of a secondary phase on a FE $Bi_4Ti_3O_{12}$·*n* ($BiCoO_3$) matrix and corona poling it afterward to improve the OER activity.

3.5. Photovoltaic Effect

Coupling of FE polarization with optical properties in ferroelectrics has received a renewed attention, trigged notably by low-band-gap FE materials suitable for sunlight spectrum absorption and original photovoltaic (PV) effect. Different from the *p*-*n* junction interfacial PV effect, the FE PV effect is a bulk phenomenon and has some out-standing advantages: i) the photo-generated carriers are separated by the depolarization field, which exists in the entire FE material, therefore, the PV is not restricted by the bandgap; ii) PV responses can be generated without forming complex junction structures; iii) the photocurrent is proportional to the polarization magnitude and the PV response can be tuned by controlling the polarization. Several typical types of FE perovskite oxides have been extensively investigated, such as $BaTiO_3$, $PbZr_{1-x}Ti_xO_3$, and $BiFeO_3$-based materials. Among them, although the depolarization field can effectively maintain the separation of the photo-generated carriers, wide bandgaps of >

3 eV make some conventional FE oxides absorb only ultraviolet light, which contains only 3.5% of solar radiation intensity. Therefore, a good FE PV material should have a narrow bandgap and a large internal electric field simultaneously, which will improve the absorption of photons and the efficiency of separating photo-generated carriers.

The band gaps of the BFTO-*n* have been determined to be about in the range of 1.28 ~ 3.1 eV, for instance, 1.28 ~ 2.12 eV in $Bi_6Fe_{2-x}Ni_xCo_xTi_3O_{18}$, 2.04 eV in BFTO-6, and 2.20–2.57 eV in $Bi_6Fe_{2-x}Co_xTi_3O_{18}$. To achieve high-efficiency PV effects in Aurivillius-phase FE oxides, the materials for BFTO-*n* with narrow band gap, robust polarization and good conductivity will be of interest. However, lots of work about PV effect for BFTO-*n* has always focused on the BFTO-4 in recent years. Kooriyattil *et al*. reported the PV effect of the BFTO-4 thin films sandwiched between ZnO:Al transparent top electrode and $SrRuO_3$ bottom electrode fabricated by PLD. This device exhibited a switchable photo-response, which is sensitive to polarization field and polarization direction, and the short-circuit photocurrent density (J_{sc}) and open-circuit voltage (V_{oc}) values are ~ 6 µA and ~ 0.14 V, respectively. Many parameters of the FE and electrode materials can affect the PV output, including remnant polarization, band gap, electrical conductivity, material/electrode interface, crystallographic orientations, microstructure, domain walls, and so on. Some attempts: band gap/interface/domain engineering) can be made to enhance PV efficiency or tune PV response of the BFTO-*n*-based devices. Bai *et al*. investigated the PV behaviors regulated by band-gap and bipolar electrical cycling in Ho-doped BFTO-4 ferroelectric films, prepared via a chemical solution deposition. It was found that the PV response peak of Ho-doped BFTO-4 films shifts toward the visible region and the J_{sc} as well as V_{oc} are improved compared with the pure BFTO-4 films.

Zhu *et al*. showed the polarization-regulated PV effect in CuO/BFTO-4 films fabricated on fluorine-doped tin oxide (FTO) glass substrate. For the Au/BFTO-4/FTO and Au/CuO/BFTO-4/FTO devices, the PV effect and power conversion efficiency of the BFTO-4 was improved by the addition of the CuO buffer layer, resulted from the formed p-n junction at the CuO/BFTO-*n* interface. By applying pulse poled bias voltages of ±10 V, the J_{sc} and V_{oc} values are markedly enhanced and the switchable PV responses were observed, mainly due to the FE depolarization field. Cao *et al*. reported the PV effect for *c*-axis preferentially oriented $Bi_4NdTi_3FeO_{15}$ ceramics. The Ag/randomly oriented ceramic/ITO device exhibits larger J_{sc} and smaller V_{oc} than those of the Ag/c-axis oriented ceramic/ITO device. Bai *et al*. reported the PV effect in heterostructural $TbFe_2$/ BTFO-4 films. The PV performances were modulated by the in-situ stress driven by magnetostriction of $TbFe_2$ clusters under external magnetic fields, and the J_{sc} and V_{oc} values increase with the in situ stress, reaching 0.026 mA/cm^2 and 9.5 V, respectively, under a maximum in-stress of 0.075 GPa. Unfortunately, to the best of our knowledge, the reported BFTO-*n*-based devices only achieve the PV efficiency of <1%. However, using a semiconductor-based model with a charge distribution in the FE material that includes polarization surface charges, Schottky-induced space charges and screening charges in the electrodes, it has been estimated that an extremely high power conversion efficiency can be reached up to 19.5%. Tremendous efforts made to enhance the PV efficiency are needed. Besides this, the origins of PV effect in the BFTO-*n* FE materials have also attracted a lot of research enthusiasm. So far, some origins have been

proposed, such as the bulk PV effect, depolarization field driven PV effect, and domain wall theory. They all deserve further studies undoubtedly.